

Spin-memory loss due to spin-orbit coupling at ferromagnet/heavy-metal interfaces: *Ab initio* spin-density matrix approach

Kapildeb Dolui and Branislav K. Nikolić*

Department of Physics and Astronomy, University of Delaware, Newark, DE 19716-2570, USA

Spin-memory loss (SML) of electrons traversing ferromagnetic-metal/normal-metal (FM/NM), FM/heavy-metal (FM/HM) and HM/NM interfaces is a fundamental phenomenon that *must* be invoked to consistently explain large number of experiments in different branches of spintronics. However, its often surprisingly large strength, extracted by fitting experimental data to phenomenological semiclassical theory which replaces each interface by a fictitious bulk layer, is poorly understood from a microscopic quantum framework and/or materials properties. Here we employ rigorous description of an ensemble of flowing spin quantum states in terms of their spin-density matrix and its polarization vector, and combine it with density functional theory (DFT) calculations to examine the reduction of the magnitude of the polarization vector, as a quantum-mechanical measure of SML, at Co/Ta, Co/Pt, Co/Cu, Pt/Cu and Pt/Au interfaces embedded within Cu/FM/NM/Cu vertical heterostructures. In addition, we use *ab initio* Green's functions to compute spectral function and spin texture over FM, HM and NM monolayers at these interfaces and quantify interfacial spin-orbit coupling, thereby explaining the microscopic origin of SML in long-standing puzzles, such as why it is nonzero at Cu/Co interface and why it is very large in junctions containing Pt/Cu interface.

Spin-memory loss (SML) of electrons traversing an interface between a ferromagnetic metal (FM) and a normal metal (NM) affects numerous spin transport phenomena in current-perpendicular-to-the-plane (CPP) geometry, such as magnetoresistance [1, 2], spin-transfer torque in spin valves [3–5] and Josephson current [6]. In addition, SML and the corresponding partial depolarization of spin current at an interface between ultrathin layers of 3d FM and 5d heavy metal (HM) is of paramount importance for understanding of recent spin-orbit torque (SOT) [7–11] and spin-pumping-to-charge conversion [12–15] experiments. For example, neglecting the spin current absorbed at the interfaces prevents [14] accurate estimation of the spin Hall angle of HM or interfacial enhancement of Gilbert damping of FM [16]. While bulk SOC induced effects are well understood [17], microscopic details of interfacial SOC at FM/HM [18, 19], as well as FM/NM or HM/NM, interfaces and its effect on spin transport remains largely unknown [20]. For example, theoretical studies of SOT [21] often assume simplistic Hamiltonians for the interfacial SOC and, aside from a handful of studies [22, 23], standard model [24] of spin pumping due to microwave driven precessing magnetization neglects interfacial SOC (despite usage of HM layers to absorb pumped spins or generate voltage via the inverse spin Hall effect [12–15]).

Traditionally, SML at interfaces has been quantified [1, 2, 6, 14] by a phenomenological parameter δ which determines the “spin-flipping” probability at the interface, $P_{\text{sf}} = 1 - \exp(-\delta)$. The parameter δ is typically extracted [1, 2] from the measurement of CPP magnetoresistance in spin valves with multilayer insertions by using semiclassical Valet-Fert model [25] to express it in terms of the thickness d of a fictitious bulk layer and its spin-diffusion length ℓ_{sf} , $\delta = d/\ell_{\text{sf}}$. However, processes at an interface—viewed as mathematically sharp plane which

is, therefore, shorter than any charge or spin dephasing length scale that would make transport semiclassical—require quantum-mechanical description [26, 27].

A step in this direction has been undertaken very recently in Ref. [28] where δ has been connected to spin-flip transmission and reflection probabilities at an individual interface computed via *ab initio* calculations to obtain δ for NM/HM interfaces (such as Cu/Pd). This probabilities are extracted from the scattering matrix within the Landauer-Büttiker (LB) approach [27] to spin-dependent quantum transport which views propagation of electrons as a process where they experience transmission and reflection events as they propagate through the system coherently. However, the approach of Ref. [28] introduces plausibly rather than rigorously defined quantity (the so-called “spin-loss conductance”) to quantify SML which assumes that spin remains aligned along fixed axis. Conversely, in the presence of interfacial SOC electrons trade angular momentum with the atomic lattice which can lead to changes of all three components of the spin. In general, SML can be due to either interfacial SOC or noncollinear magnetic moments at the interface [29].

The *rigorous* quantum-mechanical description of spin-polarization of current, viewed as an ensemble of “flowing” spin quantum states, requires to obtain the spin density matrix [30]

$$\hat{\rho}_{\text{spin}} = \frac{1}{2}(1 + \mathbf{P} \cdot \hat{\boldsymbol{\sigma}}), \quad (1)$$

as the most general description of spin- $\frac{1}{2}$ states. Here \mathbf{P} is the polarization vector and $\hat{\boldsymbol{\sigma}} = (\hat{\sigma}_x, \hat{\sigma}_y, \hat{\sigma}_z)$ is the vector of the Pauli matrices. The 2×2 Hermitian matrix $\hat{\rho}_{\text{spin}}$ of unit trace is specified by three real parameters, and, therefore, equivalently determined by the three real numbers comprising the polarization vector $\mathbf{P} = \text{Tr}[\hat{\rho}_{\text{spin}}\hat{\boldsymbol{\sigma}}]$. Pure spin quantum states, com-

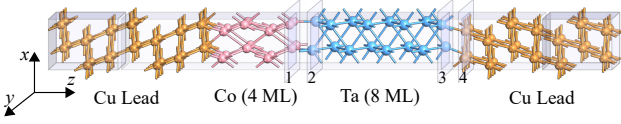


FIG. 1. (Color online) Schematic view of a vertical heterostructure for quantum transport calculations of SML, where FM/HM bilayer is sandwiched between two semi-infinite Cu(111) NM leads. Small bias voltage V_b applied between the leads injects unpolarized charge current from the left Cu lead along the z -axis in the linear-response regime. We consider FM=Co(0001) and HM=Ta(001),Pt(111). The FM layer thickness is fixed at 4 MLs, or it can be semi-infinite (by removing the left Cu lead), while HM layer thickness is varied from 0 to 5 MLs. We calculate spectral functions and spin textures on planes 1 and 2 passing through MLs of FM and HM in direct contact at the FM/HM interface, respectively, or on planes 3 and 4 passing through MLs of HM and Cu around the HM/Cu interface, respectively. The device is assumed to be infinite in the transverse direction, so that the depicted supercell is periodically repeated within the xy -plane.

prising 100% spin-polarized current, are characterized by $|\mathbf{P}| = 1$; incoherent spin states, comprising conventional unpolarized charge current, are characterized by $|\mathbf{P}| = 0$; and partially coherent [31] spin states, comprising partially spin-polarized charge current, are characterized by $0 < |\mathbf{P}| < 1$. Surprisingly enough, calculations which demonstrate how \mathbf{P} changes across FM/NM, FM/HM and HM/NM interfaces of realistic materials are lacking.

In this Letter, we combine calculation of $\hat{\rho}_{\text{spin}}$ with nonequilibrium Green functions (NEGF) [32] whose input Hamiltonian is obtained from density functional theory (DFT) theory applied to FM/HM heterostructures illustrated in Fig. 1. We consider vertical heterostructures where bilayer composed of FM=Co(0001) and HM=Ta(001),Pt(111) is attached to one or two Cu(111) semi-infinite leads. The magnetization \mathbf{m}_{Co} of the Co layer, which defines direction of \mathbf{P} for current impinging onto the interface, is aligned either parallel (i.e., along the z -axis in Fig. 1) or perpendicular (i.e., along the x -axis in Fig. 1) to the interface. The semi-infinite leads are taken into account through the corresponding *ab initio* computed self-energies [33], where unpolarized charge current is injected through the left Cu lead and spin-polarized charge current is drained through the right Cu lead. The

setup in Fig. 1 is inspired by CPP magnetoresistance-based experimental measurements [1, 2] of δ where FM/NM bilayer, whose layers are thinner than ℓ_{sf} , is inserted into Cu layer in between two FM electrodes of a spin valve, except that in our computational scheme we do not need additional right and left FM leads. It also evades the need for artificial [28] introduction of two regions—with and without SOC—within the same HM semi-infinite layer due to fact that spin current or $\hat{\rho}_{\text{spin}}$ cannot be uniquely defined along a semi-infinite lead with SOC [34].

For junctions in Fig. 1, we compute \mathbf{P} in the ballistic transport regime for current outflowing into the right Cu lead as a function of the thickness d_{HM} of the HM layer varied from 0 to 5 MLs. Thus, the parameter [14]

$$\zeta = \frac{|\mathbf{P}_{\text{NM}}^{\text{out}}|}{|\mathbf{P}_{\text{FM}}^{\text{in}}|} = \frac{|\mathbf{P}_{\text{NM}}^{\text{out}}(d_{\text{HM}} = 1 \text{ ML})|}{|\mathbf{P}_{\text{FM}}^{\text{in}}|}, \quad (2)$$

quantifies SML at FM/HM interfaces, where $|\mathbf{P}_{\text{FM}}^{\text{in}}|$ is polarization generated by an infinitely thick FM layer and $|\mathbf{P}_{\text{NM}}^{\text{out}}(d_{\text{HM}} = 1 \text{ ML})|$ is polarization of current in NM lead after insertion of 1 ML of HM. In the case of FM layers of finite thickness, we use $|\mathbf{P}_{\text{FM}}^{\text{in}}| \equiv |\mathbf{P}_{\text{NM}}^{\text{out}}(d_{\text{HM}} = 0 \text{ ML})|$. Since ζ measures the fraction of spin current absorbed at the interface, its values in Table I can be utilized as an *ab initio* boundary condition that is otherwise introduced as a phenomenological parameter $0 \leq \zeta \leq 1$ [14, 20, 23, 35]. The parameter ζ in Eq. (2) can be affected by both the FM/HM and HM/NM interfaces, as also found in realistic junctions, so we investigate the effect of the second HM/NM interface by comparing NM=Cu and NM=Au cases. Note also that $\zeta = [\cosh(\delta) + r \sinh(\delta)]^{-1}$ can be expressed in terms of measured δ and spin resistances of different layers which specify parameter r defined in Ref. [14].

By considering current in the right lead of a two-terminal junction as an ensemble (albeit nonunique [30]) of spin quantum states, the expression for $\hat{\rho}_{\text{spin}}$ was derived in Ref. [31] in terms of the transmission submatrix of the full scattering matrix as the central quantity in the LB approach to quantum transport [27]. For the most general case of injection of partially spin-polarized current from the left lead, whose spins are described by $\hat{\rho}_{\text{spin}}^{\text{in}} = p_{\uparrow}|\uparrow\rangle\langle\uparrow| + p_{\downarrow}|\downarrow\rangle\langle\downarrow|$, the spin density matrix of outgoing current in the right lead is given by [31]

$$\hat{\rho}_{\text{spin}}^{\text{out}} = \frac{e^2/h}{p_{\uparrow}(G^{\uparrow\uparrow} + G^{\downarrow\uparrow}) + p_{\downarrow}(G^{\uparrow\downarrow} + G^{\downarrow\downarrow})} \sum_{n',n=1} \begin{pmatrix} p_{\uparrow}|\mathbf{t}_{n'n,\uparrow\uparrow}|^2 + p_{\downarrow}|\mathbf{t}_{n'n,\uparrow\downarrow}|^2 & p_{\uparrow}\mathbf{t}_{n'n,\uparrow\uparrow}^*\mathbf{t}_{n'n,\downarrow\uparrow}^* + p_{\downarrow}\mathbf{t}_{n'n,\uparrow\downarrow}^*\mathbf{t}_{n'n,\downarrow\downarrow}^* \\ p_{\uparrow}\mathbf{t}_{n'n,\uparrow\uparrow}^*\mathbf{t}_{n'n,\downarrow\uparrow} + p_{\downarrow}\mathbf{t}_{n'n,\uparrow\downarrow}^*\mathbf{t}_{n'n,\downarrow\downarrow} & p_{\uparrow}|\mathbf{t}_{n'n,\downarrow\uparrow}|^2 + p_{\downarrow}|\mathbf{t}_{n'n,\downarrow\downarrow}|^2 \end{pmatrix}. \quad (3)$$

Here $\mathbf{t}_{n'n,\sigma'\sigma}$ are complex matrix elements of the transmission matrix \mathbf{t} determining probability for a spin- σ electron incoming from the left lead in the orbital state

$|n\rangle$ to appear as a spin- σ' electron in the orbital channel $|n'\rangle$ in the right lead. The zero temperature spin-resolved conductances $G^{\sigma,\sigma'}$ are given by the LB for-

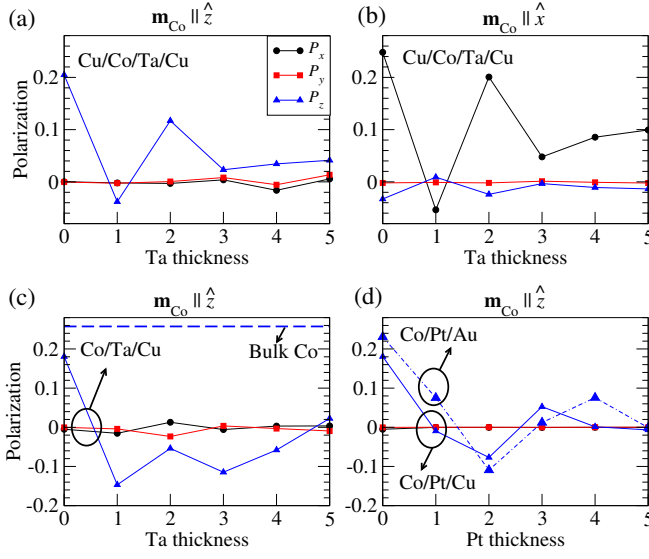


FIG. 2. The components (P_x, P_y, P_z) of the polarization vector \mathbf{P} , defined by Eq. (1), as a function of the thickness of HM=Ta,Pt layer within vertical heterostructures: (a) Cu/Co(4 ML)/Ta(n ML)/Cu with magnetization $\mathbf{m}_{\text{Co}} \parallel \hat{z}$ pointing along the direction of transport and perpendicular to the interface; (b) Cu/Co(4 ML)/Ta(n ML)/Cu with magnetization $\mathbf{m}_{\text{Co}} \parallel \hat{x}$ parallel to the interface; (c) Co/Ta(n ML)/Cu; and (d) Co/Pt(n ML)/Cu or Co/Pt(n ML)/Au (in the latter case, short dashed line plots only P_z). The horizontal dashed line in panel (c) denotes polarization $|\mathbf{P}| = P_z \simeq 0.26$ of current flowing through infinite homogeneous Co(0001) layer with its magnetization parallel to the direction of transport.

mula, $G^{\sigma, \sigma'} = \frac{e^2}{h} \sum_{n', n=1} |\mathbf{t}_{n', n, \sigma \sigma'}|^2$. Using 100% spin-polarized current injection, $p_{\uparrow} = 1.0$ and $p_{\downarrow} = 0$, Eq. (3) can be used to study SML at NM/HM interfaces in NM/HM/NM junctions which do not contain FM layer explicitly [28]. For unpolarized current injection, $p_{\uparrow} = p_{\downarrow} = 0.5$, where current can be subsequently polarized by explicitly introducing FM layer as in Fig. 1, polarization vector can be equivalently calculated [36] using $P_{\alpha} = \text{Tr}[\hat{\sigma}_{\alpha} \mathbf{t} \mathbf{t}^{\dagger}] / \text{Tr}[\mathbf{t} \mathbf{t}^{\dagger}]$.

We obtain the transmission matrix, $\mathbf{t}(E) = \sqrt{-2\text{Im} \Sigma_{\mathbf{k}_{\parallel}}^R(E)} \cdot \mathbf{G}_{\mathbf{k}_{\parallel}}(E) \cdot \sqrt{-2\text{Im} \Sigma_{\mathbf{k}_{\parallel}}^L(E)}$, using the retarded Green's function (GF) of junctions in Fig. 1

$$\mathbf{G}_{\mathbf{k}_{\parallel}}(E) = [E - \mathbf{H}_{\mathbf{k}_{\parallel}}^{\text{DFT}} - \Sigma_{\mathbf{k}_{\parallel}}^L(E) - \Sigma_{\mathbf{k}_{\parallel}}^R(E)]^{-1}. \quad (4)$$

Here $\mathbf{H}_{\mathbf{k}_{\parallel}}^{\text{DFT}}$ is DFT Hamiltonian computed for the active region composed of FM/HM bilayer with 4 MLs of the leads attached on each side, $\mathbf{k}_{\parallel} = (k_x, k_y)$ is the transverse k -vector, $\Sigma_{\mathbf{k}_{\parallel}}^{L,R}(E)$ are the self-energies [33] describing the left (L) and the right (R) semi-infinite Cu (or left Co) leads. The magnetization \mathbf{m}_{Co} of Co layer is kept either along the z -axis (i.e., direction of transport) in Fig. 1 or parallel to the x -axis (i.e., in the plane of interfaces).

Prior to DFT calculations of $\mathbf{H}_{\mathbf{k}_{\parallel}}^{\text{DFT}}$, we employ the interface builder in the VNL package [37] to construct a

TABLE I. Parameter ζ , defined in Eq. (2) to quantify SML at interfaces, for different types of junctions studied in Fig. 2. The magnetization of the Co layer is oriented along the z -axis perpendicular to the interface, except for the value in parentheses where $\mathbf{m} \parallel \hat{x}$ is in the plane of the interface.

	Cu/Co/Ta/Cu	Co/Ta/Cu	Co/Pt/Cu	Co/Pt/Au	Co/Cu	Co/Au
ζ	0.19 (0.22)	0.57	0.04	0.29	0.70	0.90

common unit cell for bilayers. In order to determine the interlayer distance and relaxed atomic coordinates, we perform DFT calculations using VASP package [38–40] with Perdew-Burke-Ernzerhof (PBE) parametrization of the generalized gradient approximation for the exchange-correlation (XC) functional and projected augmented-wave [41, 42] description of electron-core interactions. The cutoff energy for the plane wave basis set is chosen as 600 eV, while k -points were sampled at 9×9 surface mesh. The atomic coordinates are allowed to relax until the forces on each atom are less than 0.01 eV/Å, while keeping the interlayer distances d_{IL} listed in Table II fixed. Our *ab initio* quantum transport calculations are performed using ATK package [43] where we use PBE XC functional, norm-conserving pseudopotentials for describing electron-core interactions, and SG15 (medium) type local orbital basis set [44]. The energy mesh cutoff for the real-space grid is chosen as 76.0 Hartree. Transmission matrices are obtained by integrating over 251×251 k -point mesh.

The abrupt change of \mathbf{P} at different FM/HM and FM/NM interfaces, as well as along the HM layer of different thicknesses, is shown in Fig. 2. The corresponding values of the parameter ζ defined in Eq. (2) are given in Table I. An infinitely long Co layer generates $|\mathbf{P}| \simeq 0.26$, marked by dashed horizontal line in Fig. 2(c). Upon attaching Cu to Co layer, and in the absence of any HM interlayer in between them (i.e., at zero thickness of Ta or Pt layer), $|\mathbf{P}|$ reduces to $\simeq 0.18$ in Fig. 2(a) for Cu/Co(4 ML)/Cu junction or to $|\mathbf{P}| \simeq 0.20$ in Figs. 2(c) and 2(d) for semi-infinite-Co/semi-infinite-Cu junction. At first sight, it might look surprising that finite thickness Co(4 ML) layer generates larger spin-polarization of charge current than semi-infinite Co layer. However, we note that surfaces of Co (see Fig. 4(a)–(d) in Ref. [45]) and Cu (see Fig. 5(b) in Ref. 46) can host Rashba SOC enabled by inversion symmetry breaking where an electrostatic potential gradient can be created by the charge distribution at the metal/vacuum interface to confine electron wave functions into a spin-split quasi-2D electron gas [47].

TABLE II. Interlayer distance d_{IL} between metallic MLs around interfaces of junctions considered in Fig. 2.

	Cu/Co	Co/Ta	Ta/Cu	Co/Pt	Pt/Au
d_{IL} (Å)	1.86	2.06	2.05	2.05	2.18

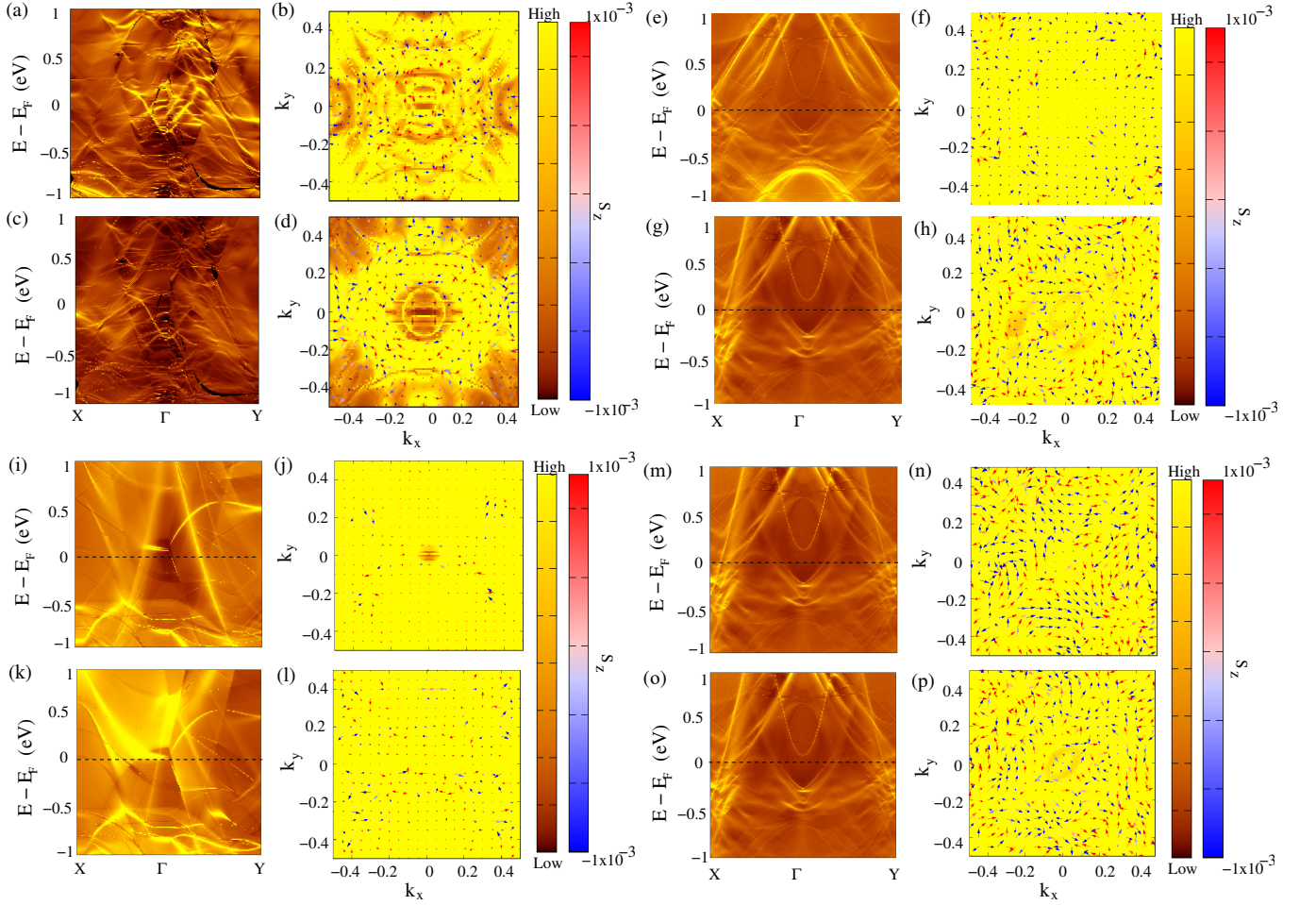


FIG. 3. Spectral function $A(E; k_x, k_y, z \in \{1, 2\})$, defined in Eq. (5), plotted along high symmetry k -path, X - Γ - Y at: (a) plane 1 in Fig. 1 passing through ML of Co; and (c) plane 2 in Fig. 1 passing through ML of Ta within Cu/Co/Ta(4 ML)/Cu junction with $\mathbf{m}_{\text{Co}} \parallel \hat{z}$. Panels (b) and (d) plot constant energy contours of $A(E - E_F^0 = 0; k_x, k_y)$ on planes 1 and 2, respectively, and the corresponding spin textures where the out-of-plane S_z component of spin is indicted in color (red for positive and blue for negative). Panels (e)–(h) show the same information on planes 1 and 2 passing through ML of Co and ML of Pt, respectively, within Co/Pt(4 ML)/Cu junction. Panels (i)–(l) show the same information on planes 1 and 2 passing through ML of Co and ML of Cu, respectively, within semi-infinite-Co/semi-infinite-Cu junction. Panels (m)–(p) show the same information on planes 3 and 4 in Fig. 1 passing through ML of Pt and ML of Cu, respectively, within Co/Pt(4 ML)/Cu junction. The units for k_x and k_y are $2\pi/a$ and $2\pi/b$ where a and b are the lattice constants along the x - and the y -axis, respectively.

Since Cu/Co(4 ML)/Cu junction is inversion symmetric, we expect zero SOC at its interfaces [7], while nonzero SOC should appear at the single interface of Co/Cu junction. This is confirmed by plotting spectral function $A(E; k_x, k_y, z)$ on ML of Co on the left side of the interface in Figs. 3(i), as well as the corresponding spin texture along constant energy contours of the spectral function at $E - E_F = 0$ in Fig. 3(j). Even larger spin texture is obtained on ML of Cu on the right side of Co/Cu interface which is, therefore, most responsible for SML at Co/Cu interface for which both zero and nonzero values of δ have been measured [2]. As anticipated, spin textures on MLs on both sides of two interfaces within inversion symmetric Cu/Co(4 ML)/Cu junction are vanishingly small. Following Ref. [45], we obtain the spec-

tral function at an arbitrary plane at position z within the heterostructure in Fig. 1 from the retarded GF

$$A(E; k_x, k_y, z) = -\frac{1}{\pi} \text{Im} [G_{\mathbf{k}_{\parallel}}(E; z, z)], \quad (5)$$

where the diagonal matrix elements $G_{\mathbf{k}_{\parallel}}(E; z, z)$ are computed by transforming Eq. (4) from local orbital to a real-space representation. The spin textures within the constant energy contours are computed from the spin-resolved spectral function.

The parameter ζ listed in Table I is much smaller for Co/Pt interface studied in Fig. 2(d) than for Co/Ta interface studied in Fig. 2(a) for the same orientation of magnetization, $\mathbf{m}_{\text{Co}} \parallel \hat{z}$. Inspection of spectral functions and spin textures around Co/Ta interface in Fig. 2(a)–(d) and around Co/Pt interface in Fig. 2(e)–(h) reveals

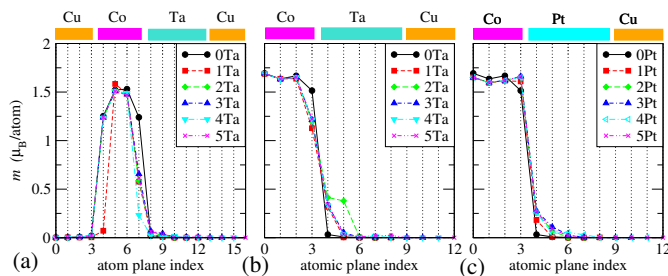


FIG. 4. Magnetic moment averaged over the total number of atoms within each ML of: (a) Cu/Co(4 ML)/Ta/Cu, (b) Co/Ta/Cu; and (c) Co/Pt/Cu junctions. The color of symbols and lines denotes different thickness of Ta or Pt HM layers, ranging from 0 to 5 MLs. Vertical dotted black lines indicate position of atomic MLs. Orange, magenta, and cyan solid boxes over the top of each panel show spatial extent of Cu, Co, Ta and Pt layers, respectively, as a guide to the eyes.

that SML is caused by both Co and Ta MLs in the former case, while it is caused mostly by Pt ML in the latter case. We emphasize that spectral function and spin textures at Co/Pt interface are quite different from those of the ferromagnetic Rashba Hamiltonian [48] often employed in calculations of SOT [21] or spin pumping in the presence of interfacial SOC [22, 23, 49]. Figure 2 also reveals that while 1 ML of HM always acts as a “spin sink,” 2 MLs can also act as a “spin source” [20] by re-polarizing charge current flowing from first to second ML of HM. Nevertheless, such “re-polarization” is eventually lost at MLs of HM further away from the FM/HM interface.

Since SML is particularly strong in Co/Pt/Cu junction in Fig. 2(d), with $\zeta \simeq 0.05$ signifying almost complete absorption of spin current by the interface, we also investigate to Co/Pt/Au junction for comparison in Fig. 2(d) and find much larger $\zeta \simeq 0.37$. Thus, this difference explains experimentally observed [1] large SML at Pt/Cu interface, which is often naively [14] attributed to interfacial diffusion and disorder. Instead, by plotting spectral functions and spin textures on the planes passing through MLs of Pt and Cu in Fig. 2(m)–(p), where spin textures on both sides of Pt/Cu interface are the largest among the cases displayed in Fig. 2, we reveal that large SML at Pt/Cu interface is due to strong interfacial SOC. Figure 2(b) also shows that for injected spins polarized parallel to the interface—i.e., $P_x \neq 0$ while the other two components of the incoming polarization vector are zero due to $\mathbf{m}_{\text{Co}} \parallel \hat{x}$ —SML reduces the magnitude of P_x while also generating non-negligible P_z out of the plane.

Finally, since change of polarization vector along HM layer of different thicknesses in Fig. 2, as well as peculiar thickness dependence of SOT observed in Co/Ta bilayers [9], can be affected by the magnetic proximity effect [19, 50]—where FM induces nonzero magnetic moments in MLs of HM layer sufficiently close to the interface—we show in Fig. 4 spatial profile of average

magnetic moment per atom across junctions studies in Fig. 2. The characteristic magnetization decay length in Pt in Fig. 4(c) is longer than in Ta in Figs. 4(a) and 4(b), where 1 ML of Ta is also capable of surprisingly large suppression of magnetic moments on the FM side for both finite and infinite thickness of the Co layer.

This work was supported by DOE Grant No. DE-SC0016380. The supercomputing time was provided by XSEDE, which is supported by NSF Grant No. ACI-1053575.

* bnikolic@udel.edu

- [1] J. Bass and W. P. Pratt Jr., *J. Phys.: Condens. Matter* **19**, 183201 (2007); J. Bass, *J. Magn. Magn. Mater.* **408**, 244 (2016).
- [2] B. Dassonneville, R. Acharyya, H. Y. T. Nguyen, R. Loloee, W. P. Pratt Jr., and J. Bass, *Appl. Phys. Lett.* **96**, 022509 (2010).
- [3] J. Grollier, V. Cros, A. Hamzic, J. M. George, H. Jaffrs, A. Fert, G. Faini, J. B. Youssef, and H. Legall, *Appl. Phys. Lett.* **78**, 3663 (2001).
- [4] S. Urazhdin, N. O. Birge, W. P. Pratt, and J. Bass, *Phys. Rev. Lett.* **91**, 146803 (2003).
- [5] S. W. Lee and K. J. Lee, *J. Korean Phys. Soc.* **55**, 1501 (2009).
- [6] M. A. Khasawneh, C. Klose, W. P. Pratt, and N. O. Birge, *Phys. Rev. B* **84**, 014425 (2011).
- [7] I. M. Miron, G. Gaudin, S. Auffret, B. Rodmacq, A. Schuhl, S. Pizzini, J. Vogel, and P. Gambardella, *Nat. Mater.* **9**, 230 (2010); I. M. Miron, K. Garello, G. Gaudin, P.-J. Zermatten, M. V. Costache, S. Auffret, S. Bandiera, B. Rodmacq, A. Schuhl, and P. Gambardella, *Nature* **476**, 189 (2011).
- [8] L. Liu, O. J. Lee, T. J. Gudmundsen, D. C. Ralph, and R. A. Buhrman, *Phys. Rev. Lett.* **109**, 096602 (2012); L. Liu, C.-F. Pai, Y. Li, H. W. Tseng, D. C. Ralph, and R. A. Buhrman, *Science* **336**, 555 (2012).
- [9] J. Kim, J. Sinha, M. Hayashi, M. Yamanouchi, S. Fukami, T. Suzuki, S. Mitani, and H. Ohno, *Nat. Mater.* **12**, 240 (2013).
- [10] X. Fan, H. Celik, J. Wu, C. Ni, K.-J. Lee, V. O. Lorenz, and J. Q. Xiao, *Nat. Commun.* **5**, 3042 (2014).
- [11] J. Sklenar, W. Zhang, M. B. Jungfleisch, W. Jiang, H. Saglam, J. E. Pearson, J. B. Ketterson, and A. Hoffmann, *J. Appl. Phys.* **120**, 180901 (2016).
- [12] E. Saitoh, M. Ueda, H. Miyajima, and G. Tatara, *Appl. Phys. Lett.* **88**, 182509 (2006).
- [13] K. Ando, S. Takahashi, J. Ieda, Y. Kajiwara, H. Nakayama, T. Yoshino, K. Harii, Y. Fujikawa, M. Matsuo, S. Maekawa, and E. Saitoh, *J. Appl. Phys.* **109**, 103913 (2011).
- [14] J.-C. Rojas-Sánchez, N. Reyren, P. Laczkowski, W. Savero, J.-P. Attané, C. Deranlot, M. Jamet, J.-M. George, L. Vila, and H. Jaffrès, *Phys. Rev. Lett.* **112**, 106602 (2014).
- [15] M. Jamali, J. S. Lee, J. S. Jeong, F. Mahfouzi, Y. Lv, Z. Zhao, B. K. Nikolić, K. A. Mkhoyan, N. Samarth, and J.-P. Wang, *Nano Lett.* **15**, 7126 (2015).
- [16] Y. Liu, Z. Yuan, R.J.H. Wesseling, A. A. Starikov, and

- P. J. Kelly, Phys. Rev. Lett. **113**, 207202 (2014).
- [17] J. Sinova, S. O. Valenzuela, J. Wunderlich, C. H. Back, and T. Jungwirth, Rev. Mod. Phys. **87**, 1213 (2015).
- [18] J.-H. Park, C. H. Kim, H.-W. Lee, and J. H. Han, Phys. Rev. B **87**, 041301 (2013); P. Moras, G. Bihlmayer, P. M. Sheverdyaeva, S. K. Mahatha, M. Papagno, J. Sánchez-Barriga, O. Rader, L. Novinec, S. Gardonio, and C. Carbone, Phys. Rev. B **91**, 195410 (2015).
- [19] S. Grytsyuk, A. Belabbes, P. M. Haney, H.-W. Lee, K.-J. Lee, M. D. Stiles, U. Schwingenschlögl, and A. Manchon, Phys. Rev. B **93**, 174421 (2016).
- [20] V. P. Amin and M. D. Stiles, Phys. Rev. B **94**, 104419 (2016); *ibid.* **94**, 104420 (2016).
- [21] P. M. Haney, H.-W. Lee, K.-J. Lee, A. Manchon, and M. D. Stiles, Phys. Rev. B **87**, 174411 (2013); K.-S. Lee, D. Go, A. Manchon, P. M. Haney, M. D. Stiles, H.-W. Lee, and K.-J. Lee, Phys. Rev. B **91**, 144401 (2015); H. Li, H. Gao, L. P. Žárbo, K. Výborný, X. Wang, I. Garate, F. Doğan, A. Čejchan, J. Sinova, T. Jungwirth, and A. Manchon, Phys. Rev. B **91**, 134402 (2015).
- [22] F. Mahfouzi, J. Fabian, N. Nagaosa, and B. K. Nikolić, Phys. Rev. B **85**, 054406 (2012); F. Mahfouzi, N. Nagaosa, and B. K. Nikolić, Phys. Rev. B **90**, 115432 (2014).
- [23] K. Chen and S. Zhang, Phys. Rev. Lett. **114**, 126602 (2015).
- [24] Y. Tserkovnyak, A. Brataas, G. E. W. Bauer, and B. I. Halperin, Rev. Mod. Phys. **77**, 1375 (2005).
- [25] T. Valet and A. Fert, Phys. Rev. B **48**, 7099 (1993).
- [26] A. Vedyayev, B. Dieny, and N. Ryzhanova, EPL (Europhysics Letters) **19**, 329 (1992).
- [27] V. S. Rychkov, S. Borlenghi, H. Jaffres, A. Fert, and X. Waintal, Phys. Rev. Lett. **103**, 066602 (2002); S. Borlenghi, V. Rychkov, C. Petitjean, and X. Waintal, Phys. Rev. B **84**, 035412 (2011).
- [28] K. D. Belashchenko, A. A. Kovalev, and M. van Schilf-gaarde, Phys. Rev. Lett. **117**, 207204 (2016).
- [29] A. B. Oparin, D. M. C. Nicholson, X.-G. Zhang, W. H. Butler, W. A. Shelton, G. M. Stocks, and Y. Wang, J. Appl. Phys. **85**, 4548 (1999).
- [30] L. E. Ballentine, *Quantum Mechanics: A Modern Development* (World Scientific, Singapore, 2014); S. Weinberg, Phys. Rev. A **90**, 042102 (2014).
- [31] B. K. Nikolić and S. Souma, Phys. Rev. B **71**, 195328 (2005).
- [32] G. Stefanucci and R. van Leeuwen, *Nonequilibrium Many-Body Theory of Quantum Systems: A Modern Introduction* (Cambridge University Press, Cambridge, 2013).
- [33] J. Velez and W. Butler, Journal of Physics: Condensed Matter **16**, R637 (2004); I. Rungger and S. Sanvito, Phys. Rev. B **78**, 035407 (2008); H. H. B. Sørensen, P. C. Hansen, D. E. Petersen, S. Skelboe, and K. Stokbro, Phys. Rev. B **77**, 155301 (2008).
- [34] B. K. Nikolić, L. P. Žárbo, and S. Souma, Phys. Rev. B **73**, 075303 (2006).
- [35] S. S.-L. Zhang and G. Vignale, Phys. Rev. B **94**, 140411 (2016).
- [36] P.-H. Chang, F. Mahfouzi, N. Nagaosa, and B. K. Nikolić, Phys. Rev. B **89**, 195418 (2014).
- [37] Virtual Nanolab (VNL) 2016.4, <http://quantumwise.com>.
- [38] Vienna Ab initio Simulation Package (VASP) 5.4, <http://www.vasp.at/>.
- [39] G. Kresse and J. Hafner, Phys. Rev. B **47**, 558 (1993).
- [40] G. Kresse and J. Furthmüller, Comput. Mater. Sci. **6**, 15 (1996).
- [41] P. E. Blöchl, Phys. Rev. B **50**, 17953 (1994).
- [42] G. Kresse and D. Joubert, Phys. Rev. B **59**, 1758 (1999).
- [43] Atomistix ToolKit (ATK) 2016.4, <http://www.quantumwise.com>.
- [44] M. Schlipf and F. Gygi, Comp. Phys. Commun. **196**, 36 (2015).
- [45] J. M. Marmolejo-Tejada, K. Dolui, P. Lazić, P.-H. Chang, S. Smidstrup, D. Stradi, K. Stokbro, B. K. Nikolić, Nano Lett. **10**.1021/acs.nanolett.7b02511 (2017).
- [46] H. Ishida, Phys. Rev. B **90**, 235422 (2014).
- [47] M. S. Bahrany, P. D. C. King, A. de la Torre, J. Chang, M. Shi, L. Patthey, G. Balakrishnan, Ph. Hofmann, R. Arita, N. Nagaosa, F. Baumberger, Nat. Commun. **3**, 1159 (2012).
- [48] N. Nagaosa, J. Sinova, S. Onoda, A. H. MacDonald, N. P. Ong, Rev. Mod. Phys. **82**, 1539 (2010).
- [49] K. Shen, G. Vignale, and R. Raimondi, Phys. Rev. Lett. **112**, 096601 (2014).
- [50] W. L. Lim, N. Ebrahim-Zadeh, J. C. Owens, H. G. E. Hentschel, and S. Urazhdin, Appl. Phys. Lett. **102**, 162404 (2013).